International Micro Air Vehicle Conference and Flight Competition (IMAV2013)
17-20 September 2013, Toulouse, France

Optimal hovering kinematics with respect to various flapping-wing shapes

Qi Wang[1], Hans Goosen[2] and Fred van Keulen[3]

[1] Delft University of Technology, Delft, The Netherlands
q.wang-3@tudelft.nl
[2] Delft University of Technology, Delft, The Netherlands
j.f.l.goosen@tudelft.nl
[3] Delft University of Technology, Delft, The Netherlands
a.vankeulen@tudelft.nl

Abstract

Flapping-wing kinematics for insect flight has been studied for decades, especially since engineers became interested in flapping-wing micro air vehicles (FWMAVs). Previous work mainly focused on understanding kinematic patterns employed by different insects from the perspective of their trajectories and aerodynamics, and on optimization of kinematic parameters to enhance the understanding. However, systematic research on the impact of different wing shapes and corresponding kinematics is incomplete. In this paper, we search for energy-efficient kinematics for hovering flight for a series of wing shapes which are described by a Beta probability density function and the shape parameter $\hat{r}_1$ (the non-dimensional radius of the first moment of wing area) to guide the wing design for FWMAVs. Three kinematic patterns are considered in the optimization: (1) fully active and harmonic kinematics for rigid wings, (2) active kinematics with linear torsion from the wing root to wing tip, (3) kinematics with passive pitching motion. We found that for the first kinematic pattern more efficient hovering flight can be achieved by the wing shape with a larger $\hat{r}_1$, a smaller frequency and no heaving motion, and linearly torsional pitching leads to more energy-efficient flight compared with kinematics with constant pitching amplitude along the leading edge. Additionally, optimal hovering kinematics with passive pitching is accompanied by heaving motion irrespective of its wing shape, which is reflected in insect flight. Although it is important to generate sufficient lift force for hovering with passive kinematics, the presence of the heaving motion dramatically increases the energy consumption.

1 Introduction

As one of the most eminent fliers, insects deeply impress us with their ultralight body, agile and highly efficient flight as well as capabilities of hovering and low-speed forward flights. Insect wings play a crucial role in their excellent flight capabilities and have fascinated biologists and engineers for centuries. Development of high-speed video cameras makes it possible to observe the trajectory of a flapping-wing in detail. Lots of experimental data of flapping-wing kinematics was collected in this way. To better understand why insects adopt certain kinematics and to find more energy-efficient kinematics for FWMAVs, sinusoidal motion was assumed most frequently to simulate the flapping-wing kinematics in experimental numerical [1, 2] and analytical [3] studies of flapping-wing aerodynamics, especially for FWMAVs [4–6]. Optimization of the flapping-wing kinematics for given flight conditions was also widely conducted. For instance, Sane and Dickinson [7] conducted experiments to determine the optimal wing kinematics of the fruit fly, Berman and Wang [8] investigated energy-minimizing

kinematics for the given morphology of fruit fly, bumblebee and hawkmoth, and Khan and Agrawal [9] determined the optimal hovering kinematics for FWMAV by means of perturbing kinematic parameters in a sequence of experiments using a robotic flapping-wing device. Comparing those observed or optimized results for different insects with different morphologies, there exists a diversity of kinematic parameters, stroke plane pattern, flapping frequency and amplitude.

As the easily accessible aspect of insects wings, the wing morphology was studied systematically and thoroughly by several biologists [10–12]. A quarter-ellipse was widely used by researchers to represent the wing shape of insects like the fruit fly [13], bumblebee [14] and hawkmoth [8, 15]. In the paper of Ellington [10], the Beta probability density function (BPDF) was proposed to describe wing shapes based on experimental data of different insects' morphological parameters. However, no further study was done to explore the effect of wing shape on the optimal kinematics for hovering flight. In this work, a quasi-steady aerodynamic model [8] is used to estimate the aerodynamic loads and power requirement for hovering flight. To minimize the power consumption while producing sufficient lift force for hovering flight with harmonic kinematics and BPDF defined shapes, we employ a hybrid optimization method, i.e., a stochastic global optimization method based on the subset simulation algorithm [16, 17] for the rough solution and a gradient-based optimization method for the precise global solution.

This paper is organized as follows. In the second section, the morphological description of the wing model is given. In the third section, a aerodynamic model for calculating aerodynamic loads and power consumption and three related coordinate systems are introduced. In the fourth section, the detailed kinematics and optimization model are described. Three hovering kinematic patterns, including fully active flapping kinematics, kinematics with linear torsion along wing span and kinematics with passive pitching, are studied in the optimization. Finally, comparisons between optimal kinematics with different kinematic patterns are given to illustrate the effect of wing shape variation on the optimal hovering kinematics .

2 Wing Morphological Description

The morphology of flapping-wings plays an important role on generating aerodynamic forces and on flight control, especially the wing shapes and moments of inertia. Biologists have been trying to find the inherent law that governs the morphology of different insect wings for centuries, and a lot of work has been done on the data collection and analysis on the wing morphology. Among them, non-dimensional radii of the k^{th} moment of wing area were used to characterize the different wing shapes [10, 11], which is defined as,

$$\hat{r}_k = \left(\int_0^1 \hat{c}\hat{r}^k d\hat{r} \right)^{1/k}, \tag{1}$$

where $\hat{c} = c/\bar{c}$ and $\hat{r} = r/R$ are non-dimensional forms of chord length c and distance r from referenced wing chord to wing base, respectively, with $\bar{c}$ representing the average chord length and R the wing span. Ellington [10] studied wings from several species of insects, including Coleoptera, Diptera, Hymenoptera, Lepidoptera, Neuroptera and Odonata, and found that there exist strong relations between the non-dimensional radii of moments of wing area for a diverse collection of insects, even for some birds and bats. More specifically, for wings of different species studied by Ellington, $\hat{r}_1$ and $\hat{r}_2$ range from $0.4 \sim 0.6$ and $0.45 \sim 0.62$, respectively. Furthermore, $\hat{r}_2$ can be approximately expressed as a function of $\hat{r}_1$ for the same wing:

$$\hat{r}_2 = 0.929\hat{r}_1^{0.732}. \tag{2}$$

In addition, Ellington [10] proposed to use the BPDF to describe the non-dimensionalized wing shape, as in,

$$\hat{c}(\hat{r};\alpha,\beta) = \frac{\hat{r}^{\alpha-1}(1-\hat{r})^{\beta-1}}{\int_0^1 \hat{r}^{\alpha-1}(1-\hat{r})^{\beta-1}d\hat{r}}, \qquad where, \quad \alpha = \hat{r}_1\frac{\hat{r}_1-\hat{r}_2^2}{\hat{r}_2^2-\hat{r}_1^2}, \beta = (\hat{r}_1-1)\frac{\hat{r}_1-\hat{r}_2^2}{\hat{r}_2^2-\hat{r}_1^2}. \tag{3}$$

Considering the relationship between $\hat{r}_1$ and $\hat{r}_2$ in Eq.(2), the chord length of an insect wing with the wing span R and average chord length $\bar{c}$ can be simply parameterized by a single parameter, i.e.,

$$c(r;\hat{r}_1) = \bar{c}\cdot\hat{c}\left(\frac{r}{R};\hat{r}_1\right). \tag{4}$$

The hawkmoth (Manduca sexta) is one of the most studied insects by biologists and referenced by man-made FWMAVs because of its moderate size and eminent hovering capability. In this work, these morphological parameters of hawkmoth wing [18], including the span length $R = 0.0519m$, aspect ratio $AR = 2.825$, wing mass $m_w = 5.79\times10^{-5}kg$ and moment of inertia of wing $I_\phi = 2.228\times10^{-8}kg\cdot m^2$, are used as basic parameters to construct wing shapes. Figure 1 shows the real wing shape of the hawkmoth and 5 different wing shapes described by the BPDF with $\hat{r}_1 = 0.40, 0.447, 0.50, 0.55, 0.60$. The wing shape for $\hat{r}_1 = 0.447$ coincides very well with real wing shape of hawkmoth, and the slight difference between them is due to the straight leading edge for the BPDF described wing shape.

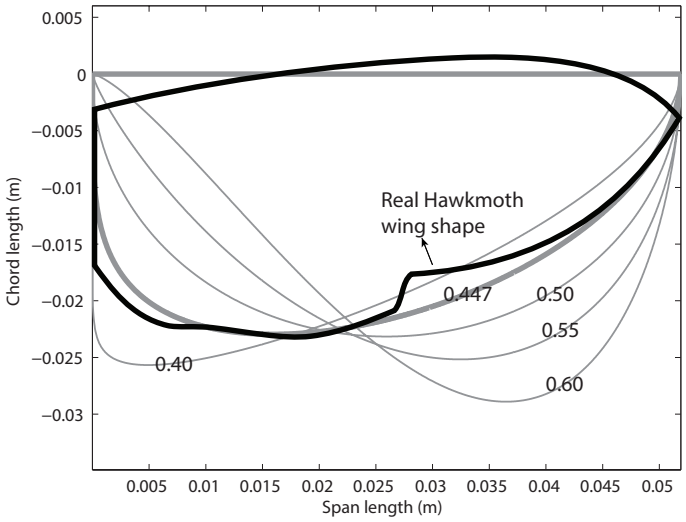

Figure 1: A series of wing shapes (gray) described by the BPDF with same R and $\bar{c}$ but different $\hat{r}_1$. A comparison is made between real hawkmoth wing shape (black) and wing shape described by the BPDF with $\hat{r}_1 = 0.447$ which was the measured value of hawkmoth wing by Willmott and Ellington [18].

Admittedly, there are limitations of the BPDF described wing shapes to completely duplicate some wing shapes because of straight leading edge and zero value at either end of the interval. Nonetheless, the wing with straight leading edge is easy to fabricate and hence a favorite of engineers, and two limitations mentioned above have negligible effects when using the quasi-steady model to calculate aerodynamic loads. Consequently, it is reasonable and convenient to use Eq.(4) to describe wing shapes with single shape parameter during the optimization.

3 Coordinate Systems and Aerodynamic Model

To optimize kinematics with different wing shapes described above, a quasi-steady aerodynamic model [8, 19, 20] is used to calculate aerodynamic loads. As the aerodynamic model uses the local pitching angles, velocities and accelerations of a wing strip to calculate the resultant loads, transformations are needed between this local coordinate system (CS) and the global CS. Therefore, these CSs related to transformations will be first described and those local information required for the calculation of aerodynamic loads will be derived as well before introducing the quasi-steady model.

3.1 Coordinate Systems

Assuming the wing is divided into many infinitesimal rigid strips, the kinematics of each strip can be described with three Euler angles, i.e. sweeping angle ϕ, heaving angle θ and pitching angle η. These angles and three involved CSs are illustrated in Figure 2. The global CS $x-y-z$ is fixed at the wing root, and its x axis coincides with the projection of the leading edge on the horizontal plane while the wing is at rest, the z axis is perpendicular to the stroke plane and upward, and the y axis is defined by the right-hand-rule. The co-rotating CS $x_c-y_c-z_c$ rotates with the wing, which is the result of three successive rotations around different axes. Three successive rotations can be denoted as three rotation matrices, i.e. $\mathbf{R}_\phi \rightarrow \mathbf{R}_\theta \rightarrow \mathbf{R}_\eta$:

$$\mathbf{R}_\phi = \begin{bmatrix} \cos\phi & -\sin\phi & 0 \\ \sin\phi & \cos\phi & 0 \\ 0 & 0 & 1 \end{bmatrix}, \mathbf{R}_\theta = \begin{bmatrix} \cos\theta & 0 & -\sin\theta \\ 0 & 1 & 0 \\ \sin\theta & 0 & \cos\theta \end{bmatrix}, \mathbf{R}_\eta = \begin{bmatrix} 1 & 0 & 0 \\ 0 & \cos\eta & -\sin\eta \\ 0 & \sin\eta & \cos\eta \end{bmatrix}. \tag{5}$$

The angular velocity of the wing can be expressed as the sum of these successive angular velocity vectors, then its coordinates expressed in the co-rotating CS are obtained by transforming three angular velocity vectors to the co-rotating CS, i.e.,

$$[\omega_{x_c}, \omega_{y_c}, \omega_{z_c}]^T = \mathbf{R}_\eta^{\mathrm{T}}\mathbf{R}_\theta^{\mathrm{T}}\mathbf{R}_\phi^{\mathrm{T}}\left[0, 0, \dot{\phi}\right]^T + \mathbf{R}_\eta^{\mathrm{T}}\mathbf{R}_\theta^{\mathrm{T}}\left[0, \dot{\theta}, 0\right]^T + \mathbf{R}_\eta^{\mathrm{T}}\left[\dot{\eta}, 0, 0\right]^T. \tag{6}$$

One strip is chosen to illustrate the velocity and acceleration expressed in the local CS $x'-y'-z'$ at its geometric center P, as shown in Figure 2. First, the absolute velocity at P expressed in the co-rotating CS can be obtained like this,

$$[v_{x_c}, v_{y_c}, v_{z_c}]^T = [\omega_{x_c}, \omega_{y_c}, \omega_{z_c}]^T \times \left[r, 0, -\tfrac{1}{2}c(r;\hat{r}_1)\right]^T \tag{7}$$

where v_{z_c} and $-v_{y_c}$ are exactly velocity components $v_{x'}$ and $v_{y'}$ in the local CS. By differentiating is Eq.(7) with time, acceleration components at P expressed in the local CS are obtained as follows:

$$a_{x'} = -r(\ddot{\theta}\cos(\eta) - \dot{\theta}\dot{\eta}\sin(\eta) + \ddot{\phi}\cos\theta\sin\eta - \dot{\phi}\dot{\theta}\sin\theta\sin\eta + \dot{\phi}\dot{\eta}\cos\theta\cos\eta), \tag{8a}$$

$$a_{y'} = r(\ddot{\theta}\sin(\eta) + \dot{\theta}\dot{\eta}\cos(\eta) - \ddot{\phi}\cos\theta\cos\eta + \dot{\phi}\dot{\theta}\sin\theta\cos\eta + \dot{\phi}\dot{\eta}\cos\theta\sin\eta) - \tfrac{1}{2}c(r)(\ddot{\eta} + \ddot{\phi}\sin\theta + \dot{\phi}\dot{\theta}\cos\theta). \tag{8b}$$

3.2 Aerodynamic Model

When a flapping-wing is accelerated or decelerated, the added mass effect has to be considered for aerodynamics analysis. Referring to the added mass for thin rectangular plate [21], the added mass

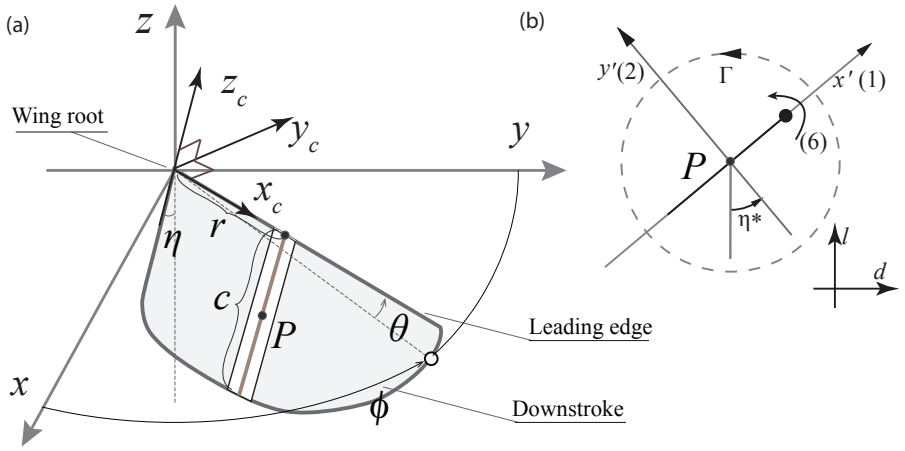

Figure 2: (a).Graph of three Euler angles and two related CSs. The gray shape represents the flapping-wing. P is the geometry center of the selected strip. The global CS, co-rotating CS are denoted as $x-y-z$ and $x_c-y_c-z_c$, respectively. It should be noted that both magnitudes of θ and η shown in the figure are negative according to the right-hand-rule. (b).Definitions of circulation (Γ), co-rotating CS $x-y-z$ and axes for added mass (modified from [19]).

tensor $\mathbf{M}$ per unit span length for the flapping wing is given as follows:

$$\mathbf{M} = \begin{bmatrix} m_{11} & m_{12} & m_{16} \\ m_{21} & m_{22} & m_{26} \\ m_{61} & m_{62} & m_{66} \end{bmatrix} = \begin{bmatrix} 0 & 0 & 0 \\ 0 & \frac{\pi}{4}\rho_{air}c^2(r;\hat{r}_1) & 0 \\ 0 & 0 & \frac{9\pi}{128}\rho_{air}c^4(r;\hat{r}_1) \end{bmatrix}, \tag{9}$$

where ρ_{air} is the density of air ($1.29kg/m^3$), and m_{ij} represents the added mass induced load in the i^{th} direction on the wing due to a unit acceleration in the j^{th} direction of the wing. Subscripts "1" and "2" denote translation along x' and y' axes, and "6" denotes the rotation around the leading edge, as shown in Figure 2(b). Based on above definition, the two-dimensional quasi-steady aerodynamic model is used to calculate aerodynamic loads for the flapping-wing by integrating loads of each strip, as in,

$$F_{x'} = \int_0^R \left[-\rho_{air} v_{y'} \Gamma - m_{11} a_{x'} + \left(\frac{c(r;\hat{r}_1)}{\bar{c}R} m_w + m_{22} \right) v_{y'} \dot{\eta} - F^v_{x'} \right] dr, \tag{10a}$$

$$F_{y'} = \int_0^R \left[\rho_{air} v_{x'} \Gamma - m_{22} a_{y'} - \left(\frac{c(r;\hat{r}_1)}{\bar{c}R} m_w + m_{11} \right) v_{x'} \dot{\eta} - F^v_{y'} \right] dr, \tag{10b}$$

$$\tau_\eta = \int_0^R \left[\tfrac{1}{4} c(r;\hat{r}_1) \rho_{air} \sqrt{v^2_{x'} + v^2_{y'}} \Gamma - m_{66} \ddot{\eta} + (m_{11} - m_{22}) v_{x'} v_{y'} - \tau^v \right] dr, \tag{10c}$$

where the quasi-steady model divides aerodynamic loads into four terms: (1) loads for an inviscid flow, (2) inertial loads, (3) loads due to Coriolis effect, (4) viscous loads. It can be found that aerodynamic forces are decomposed into components in x' and y' directions for convenience since added mass in Eq.9 is defined in the local CS. Then, the lift force L and drag force D can be easily obtained by transforming $F_{y'}$ and $F_{x'}$ by the angle $\eta^\star$, as in Figure 2(b).

To calculate the power consumption of hovering flight, the moments of inertia of the wings are required. Currently, we know the measured moment of inertia with sweeping motion I_ϕ for the wing shape with $\hat{r}_1 = 0.447$. If the mass is assumed to be uniformly distributed, the nominal moment of inertia I_ϕ^N can be calculated by $\int_0^R R^{-2} AR m_w c(r;\hat{r}_1) r^2 dr$. However, I_ϕ^N is larger than the measured I_ϕ due to inhomogeneous mass distribution for insect wings. To revise I_ϕ^N, I_θ^N and I_η^N for different wing shapes, a correction factor is introduced:

$$\lambda = \left(I_\phi / I_\phi^N\right)\big|_{\hat{r}_1=0.447}. \tag{11}$$

In addition, aerodynamic torques τ_ϕ and τ_θ can be calculated approximately by $\tau_\phi = sgn(\dot{\phi}) \int_0^R r dD$ and $\tau_\theta = -sgn(\dot{\theta}) \int_0^R r dL$. Referring to the definition in [8], the power consumption which is estimated by two terms: (1) power needed to perform rotation in a vacuum, (2) and the power used to overcome aerodynamic forces, is given in a mass-normalized form,

$$\bar{P}(t) = \Xi \left[\frac{1}{m_t} \sum_{i=\phi,\theta,\eta} \Omega_i \left(\lambda I_i^N \dot{\Omega}_i - \tau_i \right) \right], \tag{12}$$

where $\Xi[\cdot]$ is a predefined function whose value is 1 for positive value and 0 for non-positive, Ω_i denotes the angular velocity of corresponding rotation, and m_t is the total weight that wings have to bear (here we use the body weight of hawkmoth $m_t = 1.648 \times 10^{-3} kg$). For fully active kinematics, the whole flapping-wing system can not store energy according to the definition $\Xi[\cdot]$. Specially, for the passive pitching kinematics the power consumption is estimated by neglecting the term $\lambda I_\eta^N \eta\dot{\eta}$ representing the kinetic energy of pitching rotation.

4 Kinematics Description and Optimization Models

4.1 Kinematics Description

Based on the definition of Euler angles in section 3.1, sinusoidal motions are assumed for sweeping and heaving motions, as in,

$$\phi(t) = \phi_m \sin(2\pi f t), \tag{13a}$$

$$\theta(t) = \theta_m \sin(4\pi f t - \tfrac{1}{2} N\pi), \tag{13b}$$

which define the flapping motion with the figure of "∞" and "banana" shape of motion while N takes the value 0 and 1. Both shapes are commonly adopted by natural insects. For the pitching motion, three cases are considered: (1) active pitching with same amplitude along the leading edge, (2) wing torsion linearly increasing from the wing root to wing tip, (3) passive pitching mainly resulting from the combined effect of the flexible hinge at the wing root, inertia forces and aerodynamic forces.

4.1.1 Active Pitching

Active pitching here is simply defined as a sinusoidal motion, as in,

$$\eta(t) = \eta_m \sin(2\pi f t - \tfrac{\pi}{2}). \tag{14}$$

4.1.2 Linearly Increased Pitching

According to numerical simulations [22] and experimental studies [15], we know flapping insect wings exhibit increasing torsion from the wing root to wing tip. We attempt to partly figure out the reason via studying the influence of torsion on the flight efficiency with different wing shapes by assuming a linear wing torsion along the leading edge, i.e.,

$$\eta_m(r) = k_\eta r + \eta_m^{root}, \qquad 0 \le k_\eta \le \frac{\pi}{2R}, \tag{15}$$

where η_m^{root} maintains the active kinematics as described in 4.1.1 at the root, the lower bound of the slope k_η denotes the case of a constant pitching amplitude along the leading edge, and the upper bound denotes another extreme case of $\pi/2$ shift of pitching amplitudes between the wing root and wing tip. This linear approximation is close to many observed torsional shapes and allows the torsion to be described by a single parameter.

4.1.3 Passive Pitching

Another characteristic of the insect flapping-wing is the passive pitching during the stroke reversal or even the whole stoke cycle. To mimic that, a rigid wing model with a spring at wing root and with the shape described by the BPDF is assumed. Lagrange equation is used to determine the passive pitching kinematics which is governed by the spring stiffness k and non-conservative forces imposed on the wing, as in,

$$\frac{d}{dt}\left(\frac{\partial L}{\partial \dot{\eta}}\right) - \frac{\partial L}{\partial \eta} = Q, \tag{16}$$

where $L\left(\phi, \dot{\phi}, \eta, \dot{\eta}; t\right)$ denotes the Lagrangian which consists of kinetic and potential energies of flapping-wing, and Q is the sum of generalized non-conservative forces which are related to components of the non-conservative forces in global CS and transformations between global and generalized coordinate (η), as in,

$$L = K - P = \frac{1}{2}\lambda I_\eta^N \dot{\eta}^2 - \frac{1}{2}k\eta^2, \tag{17}$$

$$Q = \int_0^R \frac{\partial x}{\partial \eta} d(f_I^x + f_A^x) + \frac{\partial y}{\partial \eta} d(f_I^y + f_A^y) + \frac{\partial z}{\partial \eta} d(f_I^z + f_A^z). \tag{18}$$

The global coordinates for the geometric center of each strip along the span-wise are

$$[x, y, z]^T = \mathbf{R}_\phi \mathbf{R}_\theta \mathbf{R}_\eta \left[r, 0, -\tfrac{1}{2}c(r; \hat{r}_1)\right]^T \tag{19}$$

and two non-conservative forces, i.e, inertial forces $\mathbf{f}_I$ and aerodynamic forces $\mathbf{f}_A$, can be obtained as follows:

$$d\mathbf{f}_A = \mathbf{R}_\phi [0, dD, dL]^T = -\sin\phi dD \mathbf{e}_x + \cos\phi dD \mathbf{e}_y + dL \mathbf{e}_z, \tag{20}$$

$$d\mathbf{f}_I = \mathbf{R}_\phi [0, -r\ddot{\phi}dm, r\ddot{\theta}dm]^T = r\ddot{\phi}\sin\phi dm \mathbf{e}_x - r\ddot{\phi}\cos\phi dm \mathbf{e}_y + r\ddot{\theta}dm \mathbf{e}_z, \tag{21}$$

where the dD and dL are the drag and lift forces of a strip along the leading edge, and $\mathbf{e}_x$, $\mathbf{e}_y$ and $\mathbf{e}_z$ denote three basic vectors of the global CS. Inserting Eqs. 17 and 18 into the Lagrange equation, we get:

$$\lambda I_\eta^N \ddot{\eta} + k\eta - \frac{1}{2}\int_0^R c(r; \hat{r}_1) dD \cos\eta - \frac{1}{2}\int_0^R c(r; \hat{r}_1) dL \cos\theta \sin\eta + \frac{m_w}{2\bar{c}R}\int_0^R r c^2(r; \hat{r}_1) dr\ddot{\phi}\cos\eta - \frac{m_w}{2\bar{c}R}\int_0^R r c^2(r; \hat{r}_1) dr\ddot{\theta}\cos\theta\sin\eta = 0. \tag{22}$$

4.2 Optimization Model

Based on wing shapes described by the BPDF and analytic quasi-steady aerodynamic model, it is currently possible to conduct optimization by considering the effect of wing shapes on the optimal kinematics with different kinematic patterns. The general optimization model can be summarized as:

$$\begin{aligned} &\textbf{find} && f^*, \phi_m^*, \eta_m^*(k), \theta_m^* \\ &\textbf{minimize} && \hat{P} = \frac{1}{T}\int_T \bar{P}(t)dt \\ &\textbf{subject to} && \text{Harmonic kinematics and Wing shapes with various } \hat{r}_1. \\ & && \hat{L} = \frac{2}{Tm_tg}\int_T L(t)dt \geq 1 \\ & && 0 < f \leq 100,\ 0 < \phi_m \leq \tfrac{\pi}{2},\ 0 < \eta_m \leq \tfrac{\pi}{2},\ -\tfrac{\pi}{2} \leq \theta_m \leq \tfrac{\pi}{2} \end{aligned} \tag{23}$$

where averaged power consumption and lift force are used as objective and one of the constraints. 21 discrete values for the wing shape parameter $\hat{r}_1$ are chose from the meaningful range $0.4 \sim 0.6$ with a same interval, and independent optimization is conducted for each instance. Since kinematic optimization problems are normally nonlinear and non-convex [22], a stochastic global optimization method based on the subset simulation algorithm (SubSim optimization) [16, 17] is first used to identify the small domain where the global optimum is located. Then, the gradient-based active-set optimization algorithm by calling the *fmincon* function of Matlab® is used to find the global optimal results.

5 Results and Discussion

5.1 Active Flapping Kinematics

In order to find the most efficient active kinematics with different wing shapes both for hovering in "∞" and "banana" kinematic patterns, the SubSim optimization is used first to determine the rough global solution for all wing shapes, as shown by the four types of points in Figure 3. Then, based on results from the SubSim optimization, initial points for the gradient-based optimization are selected within $85^\circ \sim 90^\circ$, $50^\circ \sim 60^\circ$, $-3^\circ \sim 3^\circ$ and $(10 \sim 20)Hz$ for sweeping, pitching and heaving amplitudes, and frequency, respectively.

It can be found from Figure 3, that a more efficient hovering flight can be achieved by a wing shape with a larger $\hat{r}_1$ and a smaller frequency. For different wing shapes the optimal kinematics always correspond to maximal sweeping motions (90°), minimal heaving motions (0°) and moderate pitching motions ($50^\circ \sim 60^\circ$).

5.2 Torsional Wing Kinematics

To compare the optimal kinematics for torsional wing with results in Section 5.1, various wing shapes are explored to search for the most efficient f, ϕ_m, η_m^{root} and k_η. Results are given in Figure 4. Figure (a) indicates that the flapping flight with linearly torsional wing is more efficient than with constant pitching amplitude irrespective of its shape, which partly explains why insects with various wing shapes use flexible wing to generate wing torsion during flapping flight. For the torsional wing, it can be seen from Figure (b) that the optimal pitching amplitude shift between the wing root and wing tip shrinks with the increasing of $\hat{r}_1$. We attribute this to the compromise between lift generation and

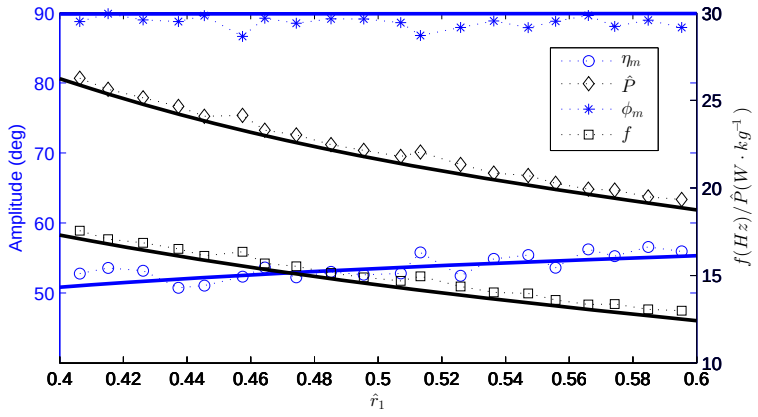

Figure 3: Optimal results for active flapping-wing kinematics for 21 wing shapes. Sets of different types of points represent the results of the SubSim optimization. Solid lines represent results of a gradient-based optimization based on those points.

energy consumption when the wing surface is more inclined to distribute at the wing tip for higher $\hat{r}_1$.

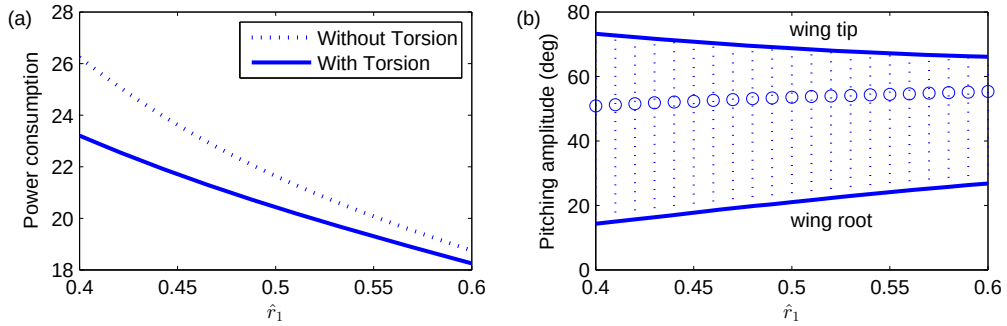

Figure 4: Comparison of optimal power consumption and pitching amplitudes between flapping flight with and without wing torsion while flapping in a horizontal stroke plane. Circles in (b) denote the optimal pitching amplitudes without wing torsion.

5.3 Passive Pitching Kinematics

Some research has been done to study contributions of inertial force and aerodynamic force to the passive pitching motion, and showed that the inertial force of the wing structure plays a more important impact on the passive pitching. Here, maintaining parameters $\phi_m = 60.3°$, $\theta_m = 3°$, $f = 26.3Hz$, $\hat{r}_1 = 0.447$ and $k = 8 \times 10^{-4} Nm/rad$, the numerical analysis based on the Lagrange equation is conducted for "∞" pattern kinematics. Passive pitching angles within first two periods are plotted in Figure 5, from which we can find the passive pitching amplitude due to inertial force is almost double that due to aerodynamic force. Furthermore, we plot results taking the variation of the wing shape

into consideration in the Figure 6. The left figure shows that amplitudes due to both sources are proportional to the value of the non-dimensional radius of the first moment of wing area $\hat{r}_1$. The second figure indicates that contributions of inertial force and aerodynamic force remain almost constant for different wing shapes described by the BPDF.

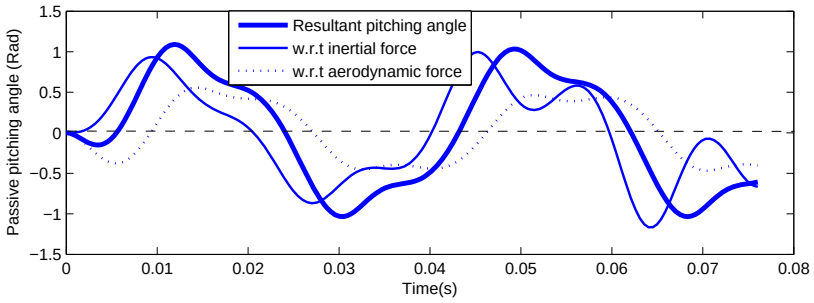

Figure 5: Contributions of inertia and aerodynamic forces to passive pitching angles in the first two cycles for "∞" pattern kinematics.

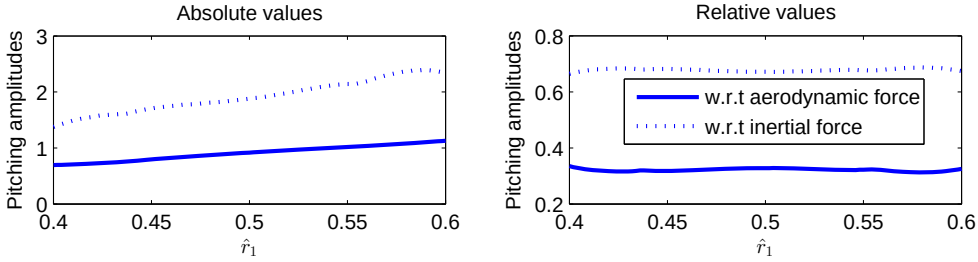

Figure 6: Contributions of inertia and aerodynamic forces to passive pitching amplitude with different wing shapes for "∞" pattern kinematics.

Due to the non-convexity of the problem and to decrease optimization time, the gradient-based optimization is not used in this case. Instead, the SubSim optimization method is used twice with relatively small number of samples to determine the global domain and to get the approximate global solution. First of all, the feasible domain for the design variables is reduced to $10 \sim 20Hz$, $4 \times 10^{-4} \sim 9 \times 10^{-4} Nm/rad$, $85° \sim 90°$ and $0° \sim 60°$ for f, k, ϕ_m and θ_m, respectively. Then, further optimization is performed with the SubSim optimization method again. As shown in Figure 7, it can be found that for wing shapes described with the BPDF the optimal spring stiffness is within $4 \times 10^{-4} \sim 6 \times 10^{-4} Nm/rad$, optimal frequency ranges from 12 to $15Hz$, and optimal heaving amplitude decreases from near 60° for $\hat{r}_1 = 0.4$ to near 0° for $\hat{r}_1 = 0.6$. The optimal sweeping amplitude is still $\pi/2$, the same as fully active optimal kinematics, which is not plotted. The passive pitching amplitude ranges from 80° to 60°, and the power consumption ranges from 80 to $30W/Kg$, both of which are larger than those for fully active optimal kinematics. The low efficiency of the passive pitching kinematics compared to active pitching kinematics can be explained by the introduction of the heaving motion, which is essential to generate enough lift force for passive pitching kinematics. On the other hand, it is worth mentioning that both the complexity and the total mass of the wing actuation mechanism are significantly reduced with passive pitching motion, and that the power required for

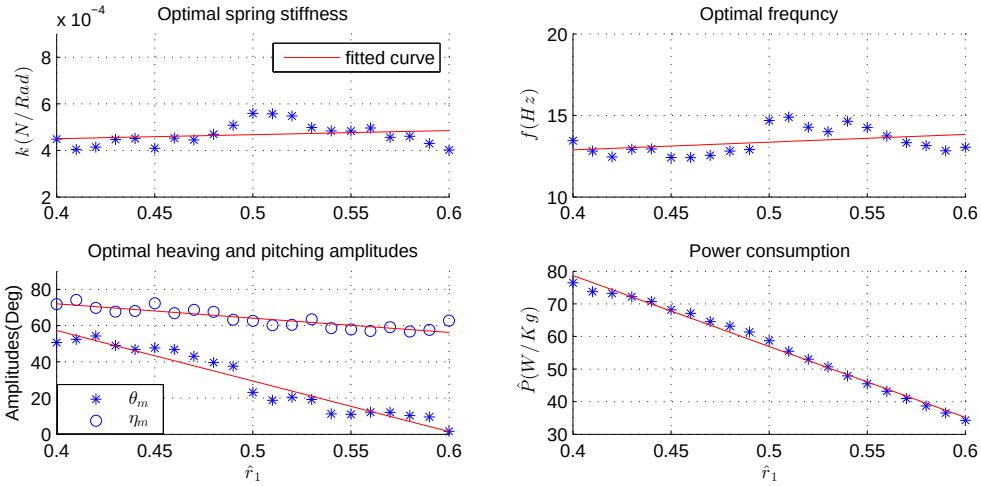

Figure 7: Optimal spring stiffness k, frequency f, heaving amplitude θ_m and corresponding passive pitching amplitude η_m and power consumption $\hat{P}$ for passive pitching kinematics with different wing shapes for "∞" pattern kinematics. These discrete results are fitted linearly to better reflect the trend.

active pitching was not considered.

6 Conclusions

Wing shapes described by the BPDF offer more options for FWMAVs compared to the quarter-ellipse wing shape or completely mimicking insect wings, and they are easy to fabricate due to the straight leading edge and smooth wing edges. From the analysis of optimization results applied to these wing shapes for hovering flight, some useful guidelines for wing design of FWMAVs are obtained. Firstly, as approximately harmonic motions are relatively easy to achieve by various actuation mechanisms especially for those based on crank-link mechanism, simply from the perspective of hovering flight, the fully actively actuated harmonic kinematics might be the most efficient scheme, while combined with a wing torsion along the span which can be achieved by deceasing the torsion stiffness. If passive flapping-wing pitching is adopted, kinematics with heaving motion is a better way to save energy. When considering the weight of the whole FWMAV which benefits from the simplicity of the actuation mechanism compared to a fully actuated mechanism, the "less" efficient passive pitching kinematics seems still favorable as a whole. Finally, for those FWMAVs mainly designed for hovering, wing shapes with larger $\hat{r}_1$ are recommended.

In the near future, more general kinematics might be considered for the optimization and the performance of kinematics with both passive pitching and torsion is also of great interest.

Acknowlegements

We would like to thank the financial support on my PhD project from China Scholarship Council and beneficial discussion with H.J. Peters.

References

[1] H. Aono, Chang-kwon Kang, Carlos E. S. Cesnik, and Wei Shyy. A numerical framework for isotropic and anisotropic flexible flapping wing aerodynamics and aeroelasticity. In *28th AIAA Applied Aerodynamics Conference*, number July, pages 1–25, Chicago, Illinois, 2010.

[2] Attila J Bergou, Leif Ristroph, John Guckenheimer, Itai Cohen, and Z Jane Wang. Fruit flies modulate passive wing pitching to generate in-flight turns. pages 1–4, 2009.

[3] S. P. Sane and Michael H. Dickinson. The aerodynamic effects of wing rotation and a revised quasi-steady model of flapping flight. *J. Exp. Biol.*, 205(8):1087–1096, April 2002.

[4] CT Bolsman. *Flapping wing actuation using resonant compliant mechanisms, an insect inspired design.* Phd thesis, Delft University of Technology, 2010.

[5] K. Y. Ma, P. Chirarattananon, S. B. Fuller, and R. J. Wood. Controlled Flight of a Biologically Inspired, Insect-Scale Robot. *Science*, 340(6132):603–607, May 2013.

[6] JP Whitney. *Design and Performance of Insect-Scale Flapping-Wing Vehicles.* Phd thesis, Harvard University, 2012.

[7] S. P. Sane and Michael H. Dickinson. The control of flight force by a flapping wing: lift and drag production. *J. Exp. Biol.*, 204(15):2607–2626, August 2001.

[8] Gordon J. Berman and Z. Jane Wang. Energy-minimizing kinematics in hovering insect flight. *Journal of Fluid Mechanics*, 582:153, June 2007.

[9] Zaeem a. Khan and Sunil K. Agrawal. Optimal Hovering Kinematics of Flapping Wings for Micro Air Vehicles. *AIAA Journal*, 49(2):257–268, February 2011.

[10] C. P. Ellington. The Aerodynamics of Hovering Insect Flight. II. Morphological Parameters. *Philosophical Transactions of the Royal Society B: Biological Sciences*, 305(1122):17–40, February 1984.

[11] T Weis-Fogh. Quick Estimates of Flight Fitness in Hovering Animals, Including Novel Mechanisms for Lift Production. *J. Exp. Biol.*, 59(1):169–230, August 1973.

[12] Robin J Wootton. Functional morphology of insect wings. *Annu. Rev. Entomol.*, 37:113–140, 1992.

[13] A. R. Ennos. Inertial and aerodynamic torques on the wings of diptera in flight. *J. Exp. Biol.*, 142(1):87–95, March 1989.

[14] R. Dudley and C. P. Ellington. Mechanics of Forward Flight in Bumblebees: I. Kinematics and Morphology. *J. Exp. Biol.*, 148(1):19–52, January 1990.

[15] AP Willmott and CP Ellington. The mechanics of flight in the hawkmoth Manduca sexta. I. Kinematics of hovering and forward flight. *J. Exp. Biol.*, 200(21):2705–2722, November 1997.

[16] Hong-Shuang Li and Siu-Kiu Au. Design optimization using Subset Simulation algorithm. *Structural Safety*, 32(6):384–392, November 2010.

[17] Qi Wang, ZhenZhou Lu, and ZhangChun Tang. A novel global optimization method of truss topology. *Science China Technological Sciences*, 54(10):2723–2729, August 2011.

[18] AP Willmott and CP Ellington. The mechanics of flight in the hawkmoth Manduca sexta. II. Aerodynamic consequences of kinematic and morphological variation. *J. Exp. Biol.*, 200(21):2723–2745, November 1997.

[19] A. Andersen, U. Pesavento, and Z. Jane Wang. Unsteady aerodynamics of fluttering and tumbling plates. *Journal of Fluid Mechanics*, 541:65–90, October 2005.

[20] Umberto Pesavento and Z. Jane Wang. Falling Paper: Navier-Stokes Solutions, Model of Fluid Forces, and Center of Mass Elevation. *Physical Review Letters*, 93(14):144501, September 2004.

[21] C.E. Brennen. A review of added mass and fluid inertial forces. Technical report, Naval Civil Engineering Laboratory, Port Hueneme, California, 1982.

[22] HJ Peters, JFL Goosen, and Fred Van Keulen. Flapping wing performance related to wing planform and wing kinematics. In *12th AIAA Aviation Technology, Integration, and Operations (ATIO) Conference and 14th AIAA/ISSM*, volume 31, pages 1–11, Indianapolis, Indiana.